RAPID MAPPING AND ASSESSMENT OF DAMAGES DUE TO TYPHOON RAI USING SENTINEL-1 SYNTHETIC APERTURE RADAR DATA

S. F. Meneses III [1,2*] and A. C. Blanco [1,2]

[1]Philippine Space Agency, University of the Philippines Diliman, Quezon City, Philippines –
serafin.meneses@philsa.gov.ph and ariel.blanco@philsa.gov.ph
[2]Department of Geodetic Engineering, UP Diliman, Quezon City, Philippines –
smmeneses@up.edu.ph and acblanco@up.edu.ph

Commission III, ICWG III/IVa

KEY WORDS: Disaster Mapping**,** Disaster Response, Typhoon Odette, UNITAR, UNOSAT

ABSTRACT:

Typhoon Rai has recently affected central and southern parts of the Philippines. Based on the valuation of the country's National Disaster Risk Reduction and Management Council (NDRRMC), it is estimated that the typhoon has damaged 1,700 buildings, 2 million houses, and 10 million hectares of agricultural land in the affected locations. Given the effects of the typhoon, in terms of the extent of the area where it has caused destruction, the tremendous economic losses due to its incurred damages, and to the number of people affected by it, it became necessary to create rapid damage assessment maps that could provide the needed geospatial information to emergency responders so they can prioritize areas of most concern. In this effort, Sentinel-1 synthetic aperture radar (SAR) imagery was used due to the data's temporal resolution (i.e., pre- and post-disaster images are available), relative independence from atmospheric conditions (i.e., unaffected by cloud cover), and open-access availability (i.e., data can be readily downloaded after the typhoon). Complex coherence correlation from stacks of pre- and post-disaster SAR images were analyzed for change detection in order to create the rapid damage assessment maps. In order to validate the results, ancillary data (i.e., aerial photos, local reports, and UNITAR / UNOSAT damage tags and maps) were used to qualitatively and quantitatively assess the maps. Upon analysis, we found that there is good correspondence between the SAR-derived maps and the aerial photos/UNITAR maps and that the damage tags by UNITAR / UNOSAT would match the rapid damage assessment maps to up to 93% if the correlation threshold is set to 0.5 and if the damage classification is set to just two levels (i.e., "damaged" and "not damaged"). It is deemed that the resulting maps of this research will be useful in the on-going efforts to rehabilitate the affected areas of Typhoo Rai. Future work includes further ground validation efforts and use of other datasets and methods in deriving the rapid damage assessment maps.

1. BACKGROUND

1.1 Introduction

Typhoon Rai, locally known as Odette, was a category 5 typhoon that has recently devastated several municipalities and cities in central and southern Philippines. The typhoon has brought tremendous damages in residential, agricultural, and industrial areas amounting to about PhP 11.5 bn (approximately € 200 million) in economic losses. The typhoon affected around 135,000 ha of crops and around 2 million infrastructures as estimated by the Philippines' National Disaster Risk Reduction and Management Committee (NDRRMC, 2022).

Part of the country's relief response to the typhoon is the creation of damage assessment maps as aid to the first responders on the ground. These maps are used to estimate the extent of the damages caused by Typhoon Rai and are important components to the ongoing rehabilitation efforts by the national and local government units. Given the travel restrictions brought about by the COVID-19 pandemic that limits the conduct of field mapping activities, the use of remote sensing for damage assessment has been a viable and practical option. This is due to the fact that satellite-based remotely-sensed data typically covers wide swaths of areas and are usually temporally available for both pre- and post-disaster analysis.

The use of remotely-sensed data has long been used for damage mapping and assessment caused by various disasters. For [1]example, optical, synthetic aperture radar (SAR), and light detection and ranging (LiDAR) has been used to map damages caused by earthquakes, landslides, explosions, tsunamis, typhoons, and floods (Van Westen, 2020; Agapiou, 2020). Optical imagery, while intuitive to use (i.e., covers the visual spectrum) and offers medium to very high spatial resolution, are generally affected by environmental and atmospheric conditions (i.e., sunlight, haze, cloud cover) (Ge, et. al., 2020; Plank, 2014). This limits their use in rapid emergency response mapping due to typhoons wherein the terrain is usually covered by clouds and haze. SAR imageries on the other hand, while generally less intuitive to visually interpret due to its viewing geometry and sensing characteristics, are generally not affected by cloud cover, haze, and rainfall (Van Westen, 2020; Plank, 2014). This renders SAR datasets advantageous to use in rapid damage mapping and assessment especially when the disasters are due to typhoons and rainfall. It is for this reason that the focus of this research would be on the use of SAR data to derive rapid damage proxy maps.

For this study, Sentinel-1 SAR datasets have been utilized by the Philippine Space Agency (PhilSA) (https://philsa.gov.ph/) to map possible locations of damaged built-up areas along the path of Typhoon Rai. This was done by stacking intensity coherence maps derived from Sentinel-1 SAR data and deriving their differences through change detection. It is hoped to be shown in

---

* Corresponding author

this study that the use of SAR data is a practical option in rapid disaster response mapping, especially for typhoons, as SAR data is generally not affected by significant cloud cover that are typically present during and after storms. This study also examined the potential of SAR data for assessing the severity of the damages by quantitatively comparing the rapid damage assessment maps to damage tags from United Nations Institute for Training and Research (UNITAR) and United Nations Satellite Center (UNOSAT).

1.2 Study Area

Study areas identified for this research are select municipalities and cities where Typhoon Rai passed during its course within the Philippine area of responsibility (PAR), namely, municipalities located in Bohol, Palawan, Dinagat, Negros, Leyte, and Siargao islands (Fig. 1).

These study areas were chosen due to the following factors: (a) estimated economic impact of the Typhoon to the location from local government units (LGU), news, and other sources, (b) extent of estimated damages by the NDRRMC, (c) availability of Sentinel-1 data that is near the time when the typhoon passed through, and (d) availability of other ancillary datasets such as the maps and shapefiles generated by the UNITAR and UNOSAT (UNITAR, 2022).
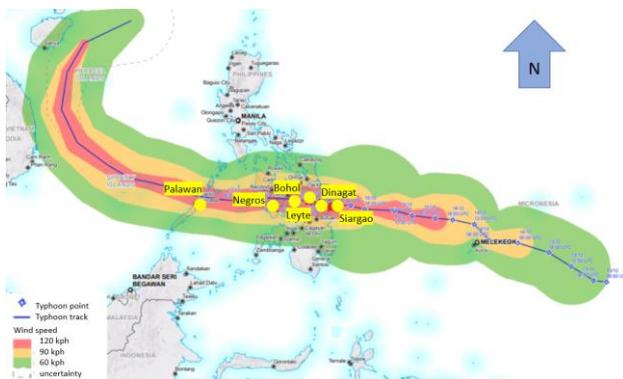
Figure 1. Path of Typhoon Rai which affected areas in the central and southern Philippines. Points indicate location map of the study areas (i.e. selected municipalities in Palawan, Negros, Bohol, Leyte, Dinagat, and Siargao). Adapted from (OCHA, 2022).

1.3 Data Sources

Sentinel-1 data used in this study were downloaded from the Scihub Copernicus website (https://scihub.copernicus.eu/dhus/#/home). Additional supporting datasets such as very high resolution (VHR) images from the International Charter Space and Major Disasters ((https://disasterscharter.org/) and preliminary damage assessment maps from UNOSAT / UNITAR (https://unitar.org/maps) were also used.

2. METHODOLOGY

2.1 Related works

Downstream remotely-sensed data has long been used for damage assessment after catastrophic events. For example, very-high resolution (VHR) optical data are traditionally used as both pre-event reference maps for pre-disaster analysis and as post-event damage maps resources through various classification methods (Brunner, et. al., 2010), image enhancement, texture analysis and creation of a variety of spectral indices (Dong and Shan, 2013). VHR optical imageries are also used for visual interpretation after explosions (Agapiou, 2020), earthquakes (Dong and Shan, 2013), and typhoons (UNITAR, 2022). However, images from passive remote sensing are prone to limitations caused by cloud cover, haze, smog, and other environmental factors which limit their applications especially when rapid response is needed (Brunner, et. al., 2010; Dong and Shan, 2013; Plank, 2014).

SAR imagery, as opposed to VHR optical images, are generally not affected by atmospheric and environmental factors (i.e. cloud cover, rain, sun illumination, etc.). This renders this datatype suitable for emergency rapid response mapping in times of calamites and catastrophic events where temporal availability is of utmost importance (Ge, et. al., 2020; Brunner et. al., 2010).

Plank (2014) gave a comprehensive review of SAR applications as used in rapid damage assessment mapping; the author enumerated the numerous studies and research that had used multi-temporal SAR data from various satellites such as ALOS PALSAR, ENVISAT, Radarsat, TerraSAR-X, and ERS. A similar study by Ge, et. al. (2020) pointed out that damage assessment mapping using SAR generally falls within three categories: (1) by using SAR interferometric complex coherence, (2) through intensity correlation coefficient, or (3) a combination of both techniques alongside polarimetric considerations. Previous studies (Ge, et. al., 2020; Hoffmann, 2007; Plank, 2014) have shown that there is good correlation between SAR-derived damage maps based on complex coherence and damage maps from VHR optical imageries and ground-truth photographs. Since the qualitative and quantitative analysis of the SAR-derived rapid damage assessment maps of this research will use VHR optical images, aerial photos from site surveys, and damage tags from UNITAR/UNOSAT as ancillary data, the rapid damage block-level mapping based on complex coherence shall be the focus of this study.

2.2 SAR Data Processing

Fig. 2 shows the data processing methodology employed in this study. First, at least three Sentinel-1 SLC images were downloaded and pre-processed. It is recommended that two images before the calamity be used along with another one taken after the typhoon. The two pre-disaster SAR images are then co-registered and stacked together. The same process is applied to the pre-disaster SAR image taken near the date when the typhoon passed over the study area and to the post-disaster SAR image.

In order to minimize noise (i.e., speckles), a noise reduction algorithm is applied (i.e., multi-look). After which, complex coherence estimation γ (Eq. 1) is then carried out to compute how correlated the pixels between the master and slave images are (Hanssen, 2002).

$$\gamma = \frac{E\{y_1 y_2^*\}}{\sqrt{E\{|y_1|^2\}E\{|y_2|^2\}}}, \tag{1}$$

where
$E\{\} $ = expectation ensemble averaging operator
y_1, y_2 = pre- and post- SAR stacks
$*$ = complex conjugate operation

Complex coherence estimated from interferometric SAR image stacks is based on the idea that changes on land cover (i.e.

collapse of buildings, falling of trees, etc.) influences the coherence between pre- and post-disaster images (Matsuoka and Yamazaki, 2004). Once complex coherence estimation is done for both the pre-disaster image pair and pre- and post-disaster image stacks, change in complex coherence ρ is estimated by applying a change detection algorithm shown by Eq. 2.

$$\rho = \log\left(\gamma_{pre}\right) - \log\left(\gamma_{post}\right), \quad (2)$$

where γ_{pre} and γ_{post} are the pre- and post- complex coherence estimates from the SAR image stacks described in Fig. 2 and Eq. 1.
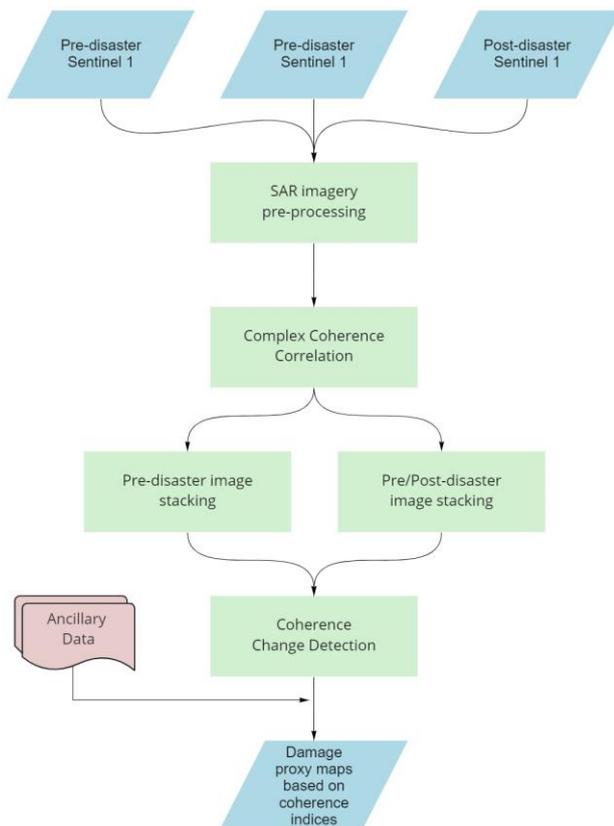
Figure 2. An overview flowchart of the processing steps used in this study wherein two-pairs of SAR images with short baselines were used to generate intensity correlation images which are then compared for change detection.

Damage estimate visualization was derived using the average coherence index table from (Hoffman, 2007) where the ratio of complex coherence given by Eq. 2 was used to estimate if the block area is severely damaged (i.e. $\rho \geq 2.5$), significantly damaged ($2.5 > \rho \geq 2.0$), or lightly damaged ($2.0 > \rho \geq 1.5$) (see Table 1).

Potential Damage Map Legend	Change ratio range	Damage approximation
	$2.0 > \rho \geq 1.5$	Light damage
	$2.5 > \rho \geq 2.0$	Moderate damage
	$\rho \geq 2.5$	Severe damage

Table 1. Rapid damage map legend based on log ratio of complex coherence from stacked SAR data.

In addition to the detected coherence change in the SAR image stacks, ancillary data from other sources such as local aerial surveys, news reports, Philippine government-led post damage needs assessments (NDRRMC, 2022), and international damage mapping efforts (UNITAR, 2022) were used to generate the final rapid damage assessment maps.

As can be seen, the processing methodology used in this study is similar to those discussed in Arciniegas, et. al., (2007), Plank (2014), Agapiou (2020) and Hoffmann (2007) wherein damage proxy maps based on complex coherence maps were derived from SAR imageries to estimate damages in built-up areas caused by disasters such as cyclones, typhoons, floods, landslides, and earthquakes.

3. RESULTS AND DISCUSSION

3.1 Rapid Damage Assessment Maps

3.1.1 Qualitative Assessment, UNITAR / UNOSAT maps: Visual comparison of derived damage assessment maps against those created by UNITAR / UNOSAT (UNOSAT, 2022) are shown in Figs. 3 – 7. It can be seen that the rapid damage assessment maps derived using Sentinel-1 were able to capture the extent of damaged areas in the study sites, namely, Bohol, Palawan, Negros, Leyte, and Siargao (Fig. 1). Post-disaster VHR optical images used by UNITAR / UNOSAT were from the Disasters Charter (The International Charter Space and Major Disasters, 2021).

Based on Figs. 3 -7, it can be surmised that the SAR-derived rapid assessment maps were able to indicate potentially damaged areas that have also been visually identified as damaged locations by using VHR optical images by UNITAR / UNOSAT. For example in Fig. 3, it can be seen in the VHR optical images that a portion of the northern part of the Talibon Port was severely damaged by the typhoon. Given the red hues over the same area in the SAR-derived map, it can be clearly seen that the damage at the port was also detected by the SAR-derived damage map. Also, while the focus of this study is on damages at built-up areas only, it can be seen in Figs. 5 – 7 that the SAR-derived rapid damage assessment maps were also able to detect damages in vegetated areas. For example, it can be seen in the VHR optical images in Fig. 6 that the trees inside the Napanto Elementary School were damaged by the typhoon and that this information was also detected using SAR imagery. While the detection of typhoon damage to vegetation is not the focus of this study, it is suggested that further studies be conducted about this in future works.

Additionally, it is also noticeable that the SAR-derived images are given at block-level (i.e., pixel level) assessment. This means that all the captured backscatter energy from all the objects within the SAR pixel were considered in deriving the complex coherence derivation from the pre- and post-disaster image stacks. This is in contrast with the object-level damage analysis typically used when using VHR optical images wherein individual buildings, houses, and other infrastructures are considered and evaluated whether damaged or not damaged (Dong and Shan, 2013; Van Westen, 2020).
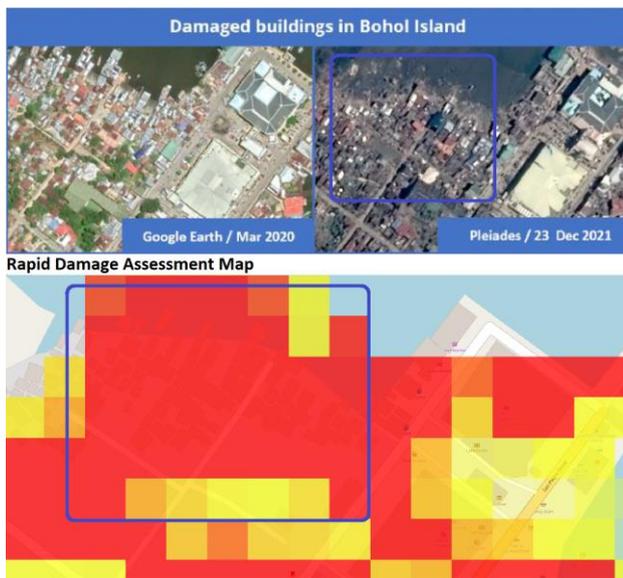
Figure 3. Sample rapid damage assessment map at Talibon, Bohol. Violet bounding box highlights the corresponding location of the damaged area caused by Typhoon Rai near Talibon Port. Basemap © OSM 2022.
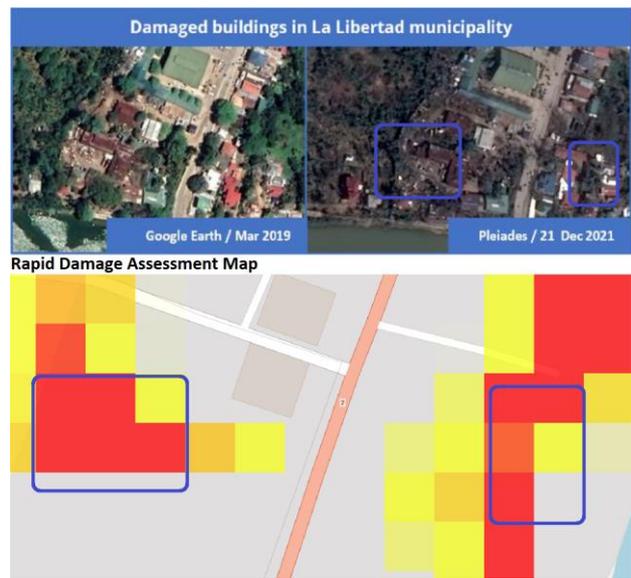
Figure 5. Rapid damage maps near La Libertad North Poblacion Primary School located in Negros Island. Bounding box indicates locations where potential damages have been identified in both optical and SAR images. Basemap © OSM 2022.
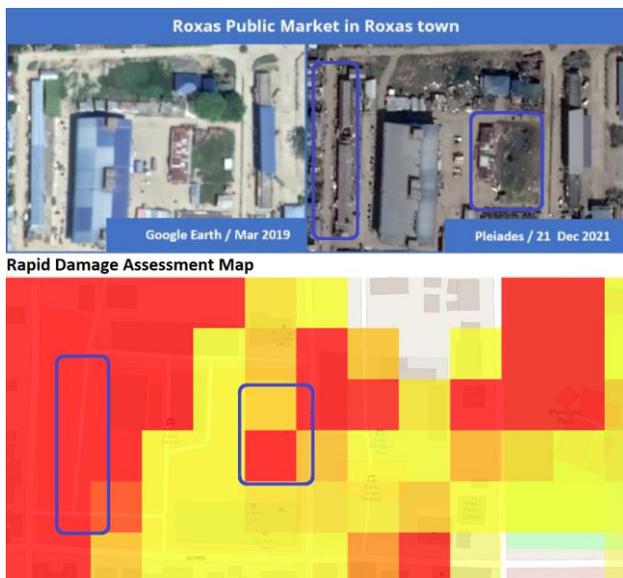
Figure 4. Damage assessment at Roxas City, Palawan. Bounding box indicates correspondence between the UNITAR/UNOSAT generated damage map and the rapid damage assessment map using SAR data. Basemap © OSM 2022.
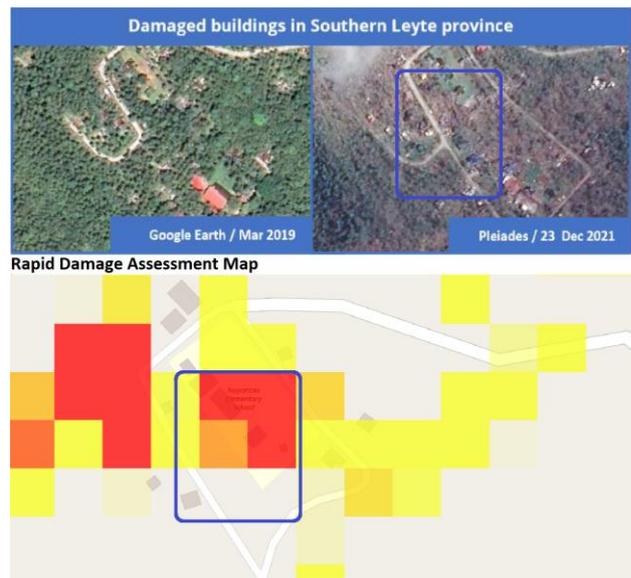
Figure 6. Rapid damage maps at Napantao Elementary School, Southern Leyte. Bounding box shows location where potential damage has been identified by both UNITAR / UNOSAT maps and by SAR-derived damage map. Basemap © OSM 2022.
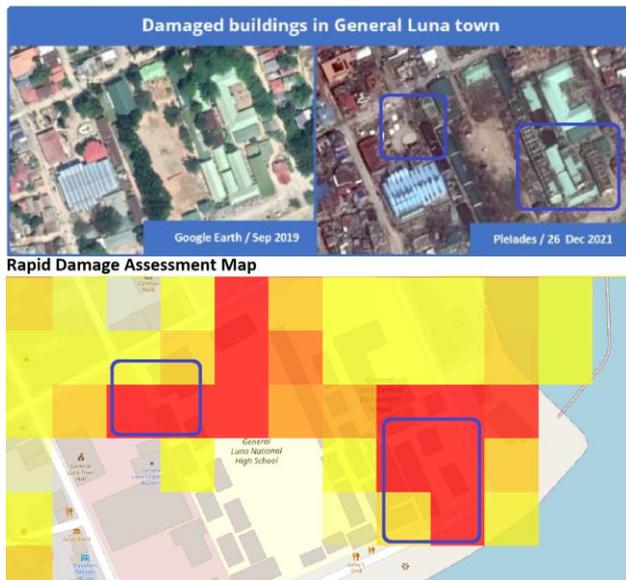
Figure 7. Rapid damage assessment maps at General Luna National High School, Siargao. Bounding boxes indicate potentially damaged roofs and buildings in the campus. Basemap © OSM 2022.

3.1.2   Qualitative Assessment, actual aerial photos: As mentioned, ground-validated ancillary data from local sources (i.e., news and government reports) were also used to qualitatively validate the generated rapid damage assessment maps. Several examples are shown in Figs. 8 - 10 wherein the SAR-derived rapid assessment maps are compared to aerial photos acquired by the Philippine Coast Guard (PCG).

Similar to the findings in Section 3.1.1, it can be seen that the SAR-derived rapid damage assessment maps were able to capture the damages at the typhoon affected areas as validated by actual aerial photographs. For example, Fig. 8 shows an aerial survey of a part of Surigao City Port where several buildings have collapsed. This damage information was also captured by the SAR-derived damage map as shown by the red hues at the bottom of the image. Likewise, Figs. 9 – 10 also show how the SAR-derived damage maps were able to detect the damages at Kangbangyo at Siargao Island and Ubay Port at Bohol Island respectively, as indicated by the red hues and their corresponding aerial survey photographs.

Figure 8. Rapid damage assessment map as validated using aerial observations from the Philippine Coast Guard. Here we can see the severely damaged infrastructure is indeed under the severely damaged block (red) in the SAR-derived damage map. Photo © PCG, 2022. Basemap © OSM 2022.
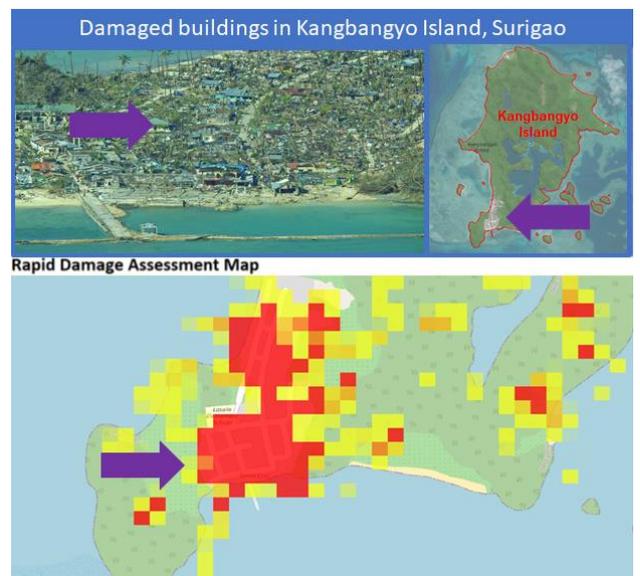
Figure 9. Comparison of the SAR-derived rapid damage assessment map and an aerial photo from PCG. Good correspondence is shown in the images. Photo © PCG, 2022. Basemap © OSM 2022.
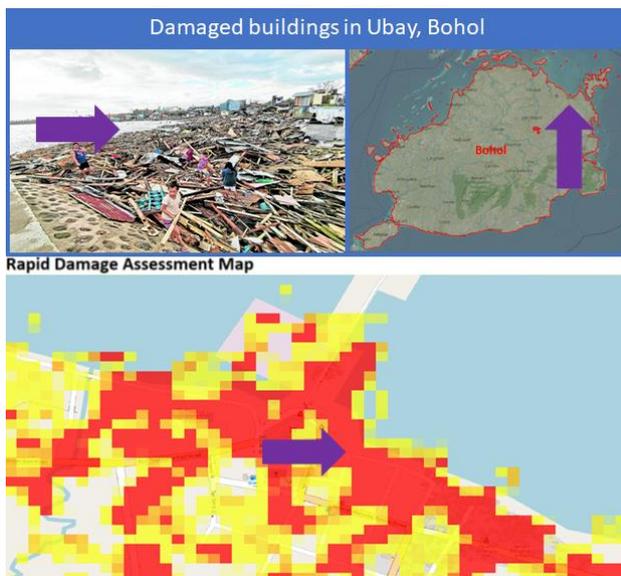
Figure 10. Good correspondence can be seen between the ground photo and the SAR-derived rapid damage assessment map at Ubay, Bohol. Photo © Inquirer.net, 2022. Basemap © OSM 2022.

3.1.3 Quantitative Assessment, UNITAR / UNOSAT damage tags: For quantitative assessment, shapefiles of damaged buildings from UNITAR / UNOSAT were used. UNITAR / UNOSAT has long been engaged in rapid damage assessment from various calamities like earthquakes, typhoons, and flooding throughout the years (UNITAR, 2022). Populated areas at ten (10) municipalities were analysed for this study. Table 2 shows the summary of the results of the quantitative comparison of the SAR-derived rapid damage maps with the damage tags created by UNITAR and UNOSAT (UNOSAT, 2022).

Location	% match			
	UN=SAR @ $\rho > 1.5$	UN=SAR @ $\rho > 0.5$	Damaged @ $\rho > 1.5$	Damaged @ $\rho > 0.5$
Gen Luna	36	41	72	100
Union	26	32	61	100
San Jose	24	27	52	76
Loreto	29	34	52	80
Pintuyan	13	13	25	50
Dakit	25	25	56	86
Ubay	57	57	85	99
Talibon	36	41	68	98

Table 2. Comparison of UNITAR / UNOSAT and SAR-derived damage tags at ten locations devastated by Typhoon Rai.

As can be seen in Table 2, a maximum of 57% (i.e. Ubay, Bohol) and a minimum of 13% (Pintuyan, Leyte) of the tagged buildings by UNITAR / UNOSAT would match the same damage categorization in the SAR-derived rapid damage assessment maps (see Table 1) if the same damage levels from UNITAR / UNOSAT would be used (i.e. potentially damaged and moderately damaged). Furthermore, it can also be noticed in Table 2 that the methodology is more sensitive to damages at study locations where there are larger built-up areas than vegetated areas (i.e. more infrastructure like houses and buildings than vegetation like trees and crops). This can be attributed to the fact that SAR decorrelation increases due the random changes in

vegetation geometry during repeat observations even if the temporal baseline is short.

If the threshold of ρ is decreased to just 0.5 (i.e. rough assumption that all changes in the complex information in the SAR interferometric pairs were caused by the typhoon and that other factors like thermal noise, topography, etc were almost completely accounted for during the pre-processing steps), we see minimal improvement on the correspondence in the UNITAR / UNOSAT and SAR-derived tags if the same levels of potentially damage and moderately damaged are used.

However, if the "labels" are disregarded and we only consider if either the buildings are damaged or not damaged, we can see improvements in the percentage of matching tags in the UNITAR / UNOSAT and SAR-derived rapid damage assessment maps as can be seen in columns three and four of Table 2. For example, if we keep the threshold value for ρ to greater than 1.5 for damaged buildings, the minimum percentage match would become 25% (i.e. at Pintuyan, Leyte) while the maximum is now at 85% at Ubay, Bohol. If the threshold for ρ is decreased to greater than 0.5, then the UNITAR / UNOSAT damage tags would match the SAR-derived tags at least 50% (still at Pintuyan, Leyte) and several would increase to 100% match correspondence in the tagged damaged locations/buildings (i.e. at General Luna and Union, Siargao).

Threshold $\rho > 1.5$	UNITAR / UNOSAT Tags		
SAR-derived	Possible Damage	Moderate Damage	Total
Possible Damage	282	1284	1566 (18%)
Moderate Damage	170	1332	1502 (11%)
Total	452 (62%)	2616 (51%)	3068

Table 3. Confusion matrix for when threshold for ρ is > 1.5. "No Damage" category from SAR-derived rapid assessment maps is disregarded since UNITAR / UNOSAT tags only use "Possible Damage" and "Moderate Damage" labels.

Threshold $\rho > 0.5$	UNITAR / UNOSAT Tags		
SAR-derived	Possible Damage	Moderate Damage	Total
Possible Damage	600	2389	2989 (20%)
Moderate Damage	170	1332	1502 (11%)
Total	770 (78%)	3721 (36%)	4491

Table 4. Confusion matrix for when threshold for ρ is > 0.5. "No Damage" category from SAR-derived rapid assessment maps is disregarded since UNITAR / UNOSAT tags only use "Possible Damage" and "Moderate Damage" labels.

Tables 3 and 4 show the confusion matrices for cases when threshold values for damage assessment are set as $1.5 \leq \rho < 2.5$ and $0.5 \leq \rho < 2.5$ for "Possible Damage", respectively. These adjustments on threshold values (see Table 1) were done in order to match the binary categorization used by UNITAR / UNOSAT in damage tagging using VHR optical images (i.e., "Possible Damage" and "Moderate Damage" only) (UNOSAT, 2022). A lower range of 0.5 from 1.5 for ρ was implemented in order to increase the sensitivity of ρ to changes in the complex coherence

of the pre- and post-disaster SAR stacks and to lessen the percentage UNITAR / UNOSAT damage tags (i.e. for both categories) being categorised as "No Damage" in the SAR-derived rapid damage assessment maps. This resulted in the reduction of the misclassification as "No Damage" of UNITAR / UNOSAT damage tags (irrespective of label) in the SAR-derived rapid damage assessment maps from 36% to 7%. $\rho \geq 2.5$ is set as "Moderate Damage" for both Tables 3 and 4 (i.e. "Severe Damage" was just re-labelled to "Moderate Damage").

As seen from Table 3, the derived User's accuracies for the "Possible Damage" and "Moderate Damage" categories are just 18% and 11% respectively while for the Producer's accuracy, the values are 62% and 51%, respectively. Overall accuracy is around 53%. Based on Table 4 (i.e., when ρ lower limit is ≥ 0.5), User's accuracies are 20% and 11% while Producer's accuracies are 78% and 36% for the "Possible Damage" and "Moderate Damage" categories respectively. Overall accuracy is just 43%. The relatively low accuracies may be explained from the fact that UNITAR / UNOSAT damage tags are "object-based" (i.e., damage tags were marked by inspecting individual built-up infrastructures or buildings from the VHR optical images) while SAR-derived damage maps are at "block-level" assessment (i.e. change in complex coherence are based from all of the multiple scatterers "inside" the SAR pixel) (Plank, 2014; Ge, et. al., 2020).

As previously done in the analysis of Table 2, in order to better assess the correspondence between the two types of rapid damage assessment maps, it is proposed that the comparison be simplified to whether the two maps classify an area of interest (AOI) as "damaged" or "not damaged". This means that the levels of damage estimate (i.e. Light, Moderate, and Severe) would be disregarded and the validation would be made solely on the basis on whether both maps classify an AOI as "damaged" or "not damaged". As seen in rows three and four of Table 5, overall correspondence (i.e. agreement on whether both datasets label AOIs as "damaged" or "not damaged") between the UNITAR / UNOSAT damage tags and SAR-derived rapid damage assessment maps are 64% and up to 94% when lower limit of ρ is set to ≥ 1.5 and ≥ 0.5 respectively. This implies that if the level of damage assessment is disregarded and the SAR-derived rapid damage assessment maps are validated solely on whether the damaged areas indicated in these maps were also tagged as damaged areas by UNITAR / UNOSAT, a relatively high overall accuracy can be observed.

Parameters	Overall % match for all locations
UN tags equals SAR categories at threshold $\rho > 1.5$	33
UN tags equals SAR categories at threshold $\rho > 0.5$	40
UN tags equals SAR categories using "damaged" / "not damaged" labels at threshold $\rho > 1.5$	64
UN tags equals SAR categories using "damaged" / "not damaged" labels at threshold $\rho > 0.5$	93

Table 5. Overall percentage matches between UNITAR / UNOSAT damage tags and SAR-derived rapid damage assessment at the eight study areas are shown in this table. First two rows show how well the categories match (i.e., whether the SAR-derived map damage estimate level matches the UNITAR / UNOSAT damage tag label). Last two rows show the percentage match when the analysis is based purely on whether the AOIs

within the study areas are tagged as "damaged" or "not damaged" regardless of the correspondence of their damage level estimates.

3.1.4 Limitations and Suggested Future Refinements: While the advantages of using SAR imagery for rapid mapping damage assessment has been discussed and emphasized in Sections 1 and 2, it is not without limitations. For example, as mentioned in Sections 3.1.1 - 3.1.3, the SAR-derived rapid damage maps derived in this study are only able to deliver block-level damage information as opposed to object-level classification possible using VHR optical images. This is primarily because of the inherent characteristics of SAR imagery, particularly on the data acquisition mode and resolution level (Ge, et. al., 2020; Plank, 2014). Another limitation of this study is that the qualitative and quantitative analysis were principally focused on damage assessment of built-up infrastructures. To refine the outputs of this study, utilization of different block-level analysis methods (Ge, et. al., 2020; Hoffmann, 2007), use of vegetation masks like normalized difference vegetation index (NDVI) to lessen the effect of of de-correlation due to vegetation (Plank, 2014), and utilization of building footprints as additional ancillary data are pipelined for future work.

3.2 Conclusions and Recommendations

Rapid damage assessment mapping is an important part of disaster response and rehabilitation activities. Maps have been traditionally used as references for rapid humanitarian aid after catastrophic events like earthquakes, tsunami, explosions, and flooding. For this study, Sentinel-1 derived block-level damage maps based on changes in complex coherence from SAR interferograms were derived to estimate damages at select built-up areas affected by Typhoon Rai.

As seen in the qualitative analysis presented in this work, SAR-derived damage proxy maps can give important information to decision makers and emergency responders about the extent and location of possibly damaged infrastructures such as houses, schools, and buildings. The derived rapid damage assessment maps show good correspondence with the actual aerial photos of damaged ports and towns and with the VHR optical image maps from UNITAR / UNOSAT and the International Charter Space and Major Disasters. Quantitative analysis has shown that by adjusting the change in complex coherence threshold to 0.5, there is 93% match between the UNITAR / UNOSAT tags and SAR-derived maps if the classification labels are set to "damaged" and "not damaged". This finding can be attributed to the fact that the maps were derived at different levels of analysis (i.e. object-level using VHR optical images and block-level when using SAR).

To further refine the results of this study, additional ancillary data can also be included, such as Global Navigation Satellite Systems (GNSS) observations at the actual sites. Maps and images from Post Disaster Needs Analysis (PDNA) from NDRRMC can also be added as another source of ground validation resource.

For future work, it is recommended that other methods using SAR (i.e., intensity correlation, polarimetry, combination of techniques, etc.) be also utilized in future rapid damage mapping activities. SAR images of different wavelengths and resolution (i.e., ALOS PALSAR, TerraSAR-X, etc.) are also being considered. Use of VHR optical imagery for damage classification and analysis using various techniques (i.e. Machine Learning, Gray Level Co-Occurrence Matrix, etc.) are also in the planned.

REFERENCES

Agapiou, A., 2020: Damage Proxy Map of the Beirut Explosion on 4th of August 2020 as Observed from the Copernicus Sensors. *Sensors*.

Arciniegas, G. A., 2007: Coherence- and Amplitude-Based Analysis of Seismogenic Damage in Bam, Iran Using ENVISAT ASAR Data. *IEEE Ttransactions on Geoscience and Remote Sensing*, 1571-1580.

Brunner, D. L., 2010: Earthquake Damage Assessment of Buildings Using VHR Optical and SAR Imagery. *IEEE Transactions on Geoscience and Remote Sensing*, 2403-2420.

Dong, L., Shan, J., 2013: A comprehensive review of earthquake-induced building damage detection with remote sensing techniques. *ISPRS Journal of Photogrammetry and Remote Sensing*, 85-99.

Ge, P., Gokon, H., Meguro, K., 2020: A review on synthetic aperture radar-based building damage assessment in disasters. *Remote Sensing of Environment*.

Hanssen, R., 2002. *Radar Interferometry Data Interpretation and Analysis.* Moscow: Kluwer.

Hoffmann, J., 2007: Mapping damage during the Bam (Iran) earthquake using interferometric coherence. *International Journal of Remote Sensing*, 1199-1216.

Matsuoka, M., Yamazaki, F., 2004: Use of Satellite SAR Intensity Imagery for Detecting Building Areas Damaged due to Earthquakes. *Earthquake Spectra,* 20(3), 975-994.

NDRRMC, 2022. National Disaster Risk Reduction and Management Committee Situational Report on Typhoon Odette. https://monitoring-dashboard.ndrrmc.gov.ph/page/situation/situational-report-for-tc-odette-2021 (13 January 2022).

OCHA, 2022. United Nations Office for the Coordination of Humanitarian Affairs, 2021. United Nations Office for the Coordination of Humanitarian Affairs (OCHA) Relief Web Path of Typhoon Rai (Odette). https://reliefweb.int/map/philippines/philippines-super-typhoon-rai-odette-path-typhoon-rai-odette-17-dec-21 (13 Jan 2022).

Plank, S., 2014: Rapid Damage Assessment by Means of Multi-Temporal SAR — A Comprehensive Review and Outlook to Sentinel-1. *Remote Sensing*, 4870-4906.

The International Charter Space and Major Disasters, 2021. Typhoon Rai in the Philippines. https://disasterscharter.org/web/guest/activations/-/article/storm-hurricane-rural-in-philippines-activation-741- (16 December 2021)

UNITAR, 2022. Assessing the Large Scale Damages by the Tropical Cyclone Rai-21 in the Philippines. https://www.unitar.org/about/news-stories/news/assessing-large-scale-damages-tropical-cyclone-rai-21-philippines (09 February 2022).

UNOSAT, 2022). The 16th of December 2021 Category 5 Tropical Cyclone RAI-21, The Philippines. Preliminary Satellite-Based Comprehensive Damage Assessment Report. Geneva: United Nations Satellite Centre (UNOSAT).

Van Westen, C. (2020). Remote Sensing for Natural Disaster Management. *Int. Arch. of Photogramm. and Remote Sens. Spatial Inf. Sci.*, *XXXIII, Part B7*, pp. 1609-1617. Amsterdam: ISPRS.